IEEE Photonics Journal
An IEEE Photonics Society Publication

Open Access

High Reflectivity YDH/SiO_2 Distributed Bragg Reflector for UV-C Wavelength Regime

Volume 10, Number 2, April 2018

Mohd Sharizal Alias, *Member, IEEE*
Abdullah A. Alatawi
Wong Kim Chong
Malleswararao Tangi
Jorge A. Holguin-Lerma, *Student Member, IEEE*
Edgars Stegenburgs
Mohammad Khaled Shakfa
Tien Khee Ng, *Senior Member, IEEE*
Abdulrahman M. Albadri
Ahmed Y. Alyamani
Boon S. Ooi, *Senior Member, IEEE*

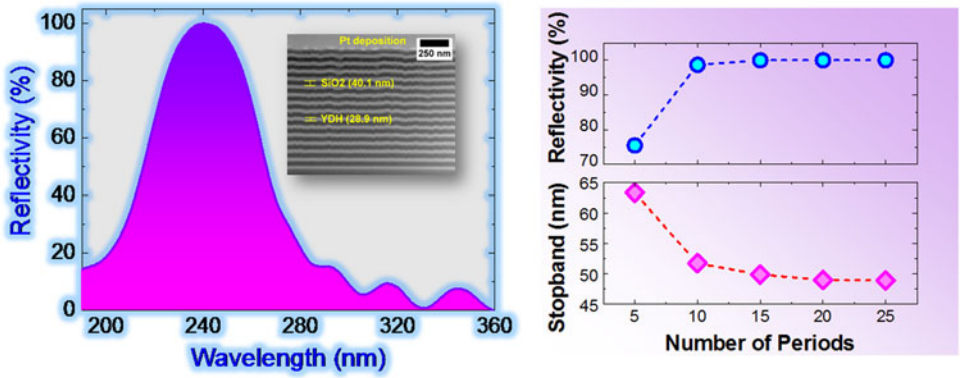

DOI: 10.1109/JPHOT.2018.2804355
1943-0655 © 2018 IEEE

High Reflectivity YDH/SiO_2 Distributed Bragg Reflector for UV-C Wavelength Regime

Mohd Sharizal Alias,[1] ***Member, IEEE***, **Abdullah A. Alatawi**,[1,3] **Wong Kim Chong**,[2] **Malleswararao Tangi**,[1] **Jorge A. Holguin-Lerma**,[1] ***Student Member, IEEE***, **Edgars Stegenburgs**,[1] **Mohammad Khaled Shakfa**,[1] **Tien Khee Ng**,[1] ***Senior Member, IEEE***, **Abdulrahman M. Albadri**,[3] **Ahmed Y. Alyamani**,[3] **and Boon S. Ooi**,[1] ***Senior Member, IEEE***

[1]Photonics Laboratory, Computer, Electrical and Mathematical Science and Engineering Division, King Abdullah University of Science and Technology, Thuwal 23955-6900, Saudi Arabia
[2]Core Labs, King Abdullah University of Science and Technology, Thuwal 23955-6900, Saudi Arabia
[3]National Center for Nanotechnology, King Abdulaziz City for Science and Technology, Riyadh 11442-6086, Saudi Arabia

DOI:10.1109/JPHOT.2018.2804355

Manuscript received December 25, 2017; revised January 24, 2018; accepted February 6, 2018. Date of publication February 12, 2018; date of current version March 1, 2018. This paper is based on the work supported in part by the King Abdulaziz City for Science and Technology under Grant KACST TIC R2-FP-008, and in part by the King Abdullah University of Science and Technology baseline funding BAS/1/1614-01-01. Corresponding author: B. S. Ooi (e-mail: boon.ooi@kaust.edu.sa).

Abstract: A distributed Bragg reflector (DBR) composed of Y_2O_3-doped HfO_2 (YDH)/SiO_2 layers with high reflectivity spectrum centered at a wavelength of ~240 nm is fabricated using radio-frequency magnetron sputtering. Before the DBR deposition, optical properties for a single layer of YDH, SiO_2, and HfO_2 thin films were studied using spectroscopic ellipsometry and spectrophotometry. To investigate the performance of YDH as a material for the high refractive index layer in the DBR, a comparison of its optical properties was made with HfO_2 thin films. Due to larger optical bandgap, the YDH thin films demonstrated higher transparency, lower extinction coefficient, and lower absorption coefficient in the UV-C regime (especially for wavelengths below 250 nm) compared to the HfO_2 thin films. The fabricated YDH/SiO_2 DBR consisting of 15 periods achieved a reflectivity higher than 99.9% at the wavelength of ~240 nm with a stopband of ~50 nm. The high reflectivity and broad stopband of YDH/SiO_2 DBRs will enable further advancement of various photonic devices such as vertical-cavity surface-emitting lasers, resonant-cavity light-emitting diodes, and resonant-cavity photodetectors operating in the UV-C wavelength regime.

Index Terms: Distributed Bragg reflector, thin films, ultraviolet.

1. Introduction

Highly reflective distributed Bragg reflectors (DBRs) in the ultraviolet (UV) wavelength regime are important for UV-based photonic devices such as vertical-cavity surface-emitting lasers (VCSELs), polariton lasers, light-emitting diodes (LEDs), photodetectors (PDs), and solar cells. DBRs can be integrated into these devices as mirrors to enhance the light amplification. Typically, a DBR

can be formed by repetitively stacking alternating high- and low-refractive index (RI) layers with the thickness of each layer corresponding to a quarter-wave of the operating wavelength. In the UV wavelength regime, group III-nitride materials (e.g., GaN/AlGaN, AlGaN/AlInN, AlGaN/AlN, and AlGaN/air), and dielectric materials (e.g., TiO_2/SiO_2, Ta_2O_5/SiO_2, HfO_2/SiO_2, and ZrO_2/SiO_2) based-DBRs have been used in the design and fabrication of UV VCSEL [1]–[3], UV edge-emitting laser [4], UV polariton laser [5], UV resonant-cavity LED [6], UV LED [7], and UV PD [8]. The advantages of group III-nitride DBRs is that they can be monolithically grown and doped with desired n- or p-type dopants required for electrical pumping. However, obtaining dislocation- and crack-free structures is challenging due to the limited crystal quality (e.g., lattice- and thermal expansion-mismatch), growth complexity (e.g., composition- and growth temperature-fluctuation), and the inadequate reflectivity (i.e., low RI contrast) of group III-nitride materials. In contrast, for dielectric DBRs, the choice of the materials and the growth method are more extensive and flexible. Highly reflective DBRs exceeding 99% reflectivity can be easily obtained within a small number of repetitions due to the high RI contrast, i.e., 10 to 15 periods typically [2], [5], compared to 30 to 50 periods for group III-nitride DBRs [9]. However, a complex device scheme, e.g., the intra-cavity design, is required to realize electrical pumping for devices using dielectric DBRs [6].

Focusing on dielectric DBRs for the UV-C regime i.e., $<$280 nm wavelength, the use of fluorides, e.g., LaF_3/AlF_3 [10] and LaF_3/MgF_2 [11]; oxide-fluoride combinations, e.g., Al_2O_3/MgF_2 [12] and Al_2O_3/AlF_3 [10]; and oxides only, e.g., Al_2O_3/SiO_2 [13] and HfO_2/SiO_2 [14], [15]; have been reported. The fluorides and oxides-fluorides based DBRs were developed for reflectivities at sub-200 nm wavelengths [10]–[12]. For operating wavelengths above 200 nm, the oxides based DBRs were used [13]–[16]. Although fluorides exhibit relatively low UV-C absorption, a high number ($>$40 pairs) of DBR periods is required due to the small RI contrast [10]. Furthermore, fluoride layers are required to be deposited at high substrate temperature to obtain stable film structural and optical properties. This condition promotes high tensile stress during the deposition due to the large thermal expansion coefficient difference between the film and the substrate, which can lead to micro-cracks for a thick DBR structure [10]. If using oxides only as in the case of Al_2O_3/SiO_2 DBR [13], around 42.5 periods were required to achieve a reflectivity of $>$99% in the UV-C regime due to insufficient RI contrast. Replacing Al_2O_3 by HfO_2 as the high RI layer for the DBR (with SiO_2 as the low RI layer) is attractive because of higher RI contrast. However, HfO_2 starts absorbing light below the wavelength of 250 nm. Therefore, most of the reported HfO_2/SiO_2 DBRs have been only designed for wavelengths above 250 nm [13]–[16]. Recently, it has been shown that the material properties of HfO_2 films can be improved by the incorporation of Y_2O_3 (also known as yttria). Compared with HfO_2 films, the Y_2O_3-doped HfO_2 (YDH) films exhibited better structural stability [17], [18], higher effective dielectric constant [19], lower leakage current density [17], and larger optical bandgap [20]–[22]. Specifically, on the optical bandgap (E_g), Noor-A-Alam *et al.* [20] and Chen *et al.* [21], [22] reported that more than 6 eV could be achieved for YDH films with a certain composition.

Here, we demonstrate a YDH/SiO_2 DBR with a reflectivity higher than 99.9% operating in the UV-C regime. This DBR exhibits a $\sim$50 nm broad stopband centered at $\sim$240 nm wavelength. Due to the high RI contrast and low absorption of the materials, the YDH/SiO_2 DBR requires only 15 periods to achieve the aforementioned reflectivity. We also compare the optical characteristics of single layer YDH and HfO_2 thin films prior to the full DBR deposition. Recently, several AlGaN-based lasers were reported for UV-C lasing at $\sim$240 nm wavelength [23]–[26]. By having such as high reflectivity around 240 nm wavelength with only 15 periods, YDH/SiO_2 DBRs can be used as a mirror for these UV-C lasers and other UV-C photonic devices.

2. Depositions of DBRs and Thin Films

The YDH/SiO_2 DBRs were deposited onto UV-grade sapphire substrates by radio-frequency (RF) magnetron sputtering. A single layer of YDH, HfO_2, and SiO_2 thin films were also deposited onto both UV-grade sapphire and silicon substrates to investigate the optical properties of these materials. All substrates were cleaned using the standard solvents-ultrasonic cleaning and dried with N_2 before being loaded into the vacuum chamber, which was initially evacuated to a base pressure

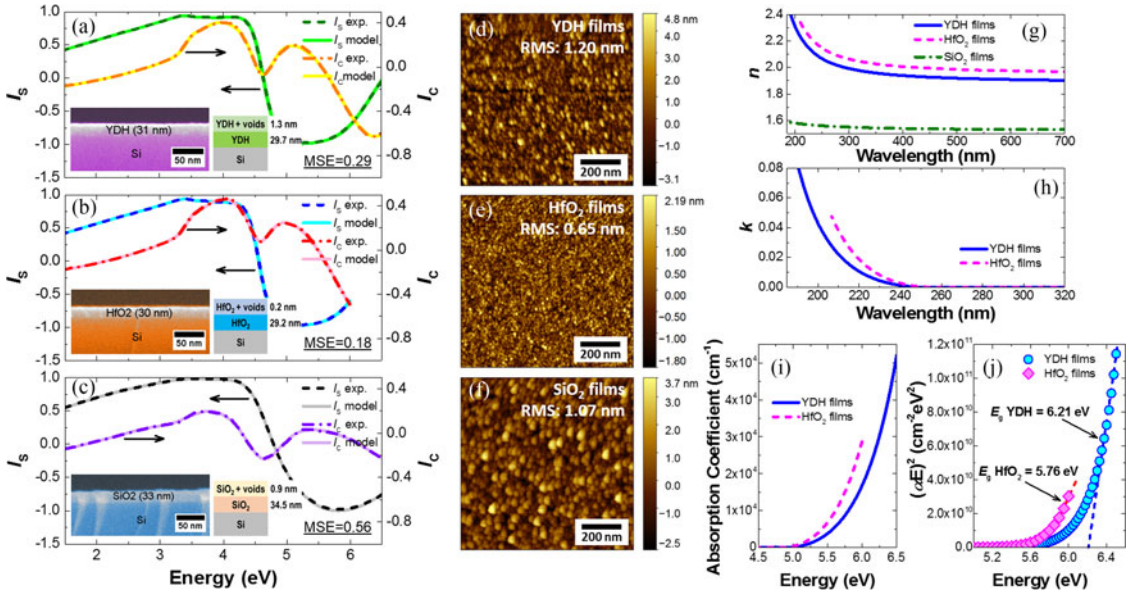

Fig. 1. Measurements and analysis of the YDH, HfO_2, and SiO_2 thin films showing (a)–(c) modeled and experimentally obtained SE spectra of each material with the SEM cross-section micrograph (left) and optical stack model (right) as insets, (d)–(f) AFM surface scan for each material with the respective RMS roughness value, (g) wavelength-dependent RI spectra, (h) wavelength-dependent extinction coefficient spectra, (i) absorption coefficient spectra, and (j) Tauc plot revealing the values of optical bandgap.

of $\sim 10^{-7}$ torr. A commercial-ready 2-inch diameter YDH target composed of $(Y_2O_3)_{0.2}(HfO_2)_{0.8}$, SiO_2 target, and HfO_2 target with a purity of 99.9%, 99.995%, and 99.95%, respectively, were used for the sputtering. The RF power applied to all targets were set to 75 W. The sputtering gas was Ar with the gas flow maintained at 25 sccm. Before the actual deposition, all targets were pre-sputtered for 10 min with the shutter above the sputter gun closed. All samples were sputtered at room temperature with a working pressure of $\sim 10^{-3}$ torr. The deposition rates were 2.4, 2.0, and 0.8 nm/min for HfO_2, YDH, and SiO_2 thin films, respectively.

3. Material Characterizations of Thin Films

To design the YDH/SiO_2 DBR, measurements using spectroscopic ellipsometer (SE) were performed to investigate the wavelength-dependent RI (n) of YDH and SiO_2 thin films, and to study the comparison of extinction coefficient (k) and E_g between YDH and HfO_2 thin films in the UV regime. The deposited thickness of all samples was fixed to $\sim$30 nm. Since the wavelength of interest is in the UV regime, a phase modulated SE was used where the signals detected are in the form of harmonics (symbolized as I_S and I_C) that can be extracted to determine the ellipsometric angles (Ψ and Δ) as a function of energy [27]. Data were acquired at an incident angle of 70° over a spectral range from 1.5 eV up to just beyond the respective E_g for each material. To extract the optical constants (n and k), film thickness, and the surface morphology information, the measured harmonics were fitted to data generated from a model representing the sample structure. For the SE modeling, the Tauc-Lorentz model [28] (which is suited for amorphous semiconductors and Kramers-Kronig consistent) was used for the YDH, HfO_2, and SiO_2 materials. A good fit to the measured data indicated by the lowest possible mean squared error (MSE) based on Levenberg-Marquardt regression algorithm is required across the measured spectral range. Fig. 1(a) to (c) show the measured versus modeled SE spectra with a good fitting obtained (nominal MSE values) for the YDH, HfO_2, and SiO_2 thin films, respectively, and show the corresponding scanning electron microscope (SEM) cross-section micrographs and optical stack models in insets. The thickness of the single YDH, HfO_2, and SiO_2 layers and the root-mean-square (RMS) roughness obtained from

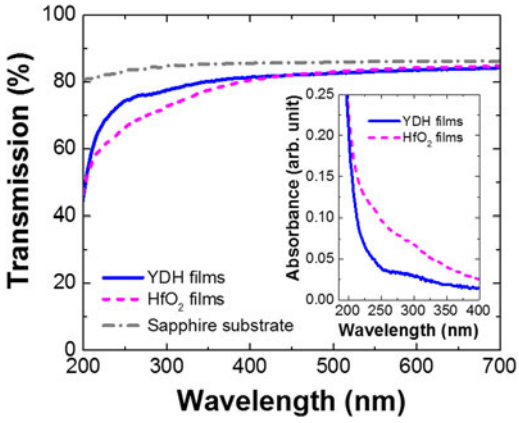

Fig. 2. Transmission spectra of the YDH and HfO_2 thin films deposited on UV-grade sapphire substrates. The inset shows the absorbance spectra for both materials in the UV regime.

the SE modeling were in good agreement with the measured cross-sectional micrographs using SEM and the surface scans using atomic force microscope (AFM). The AFM images for the YDH, HfO_2, and SiO_2 thin films are shown in Fig. 1(d) to (f), respectively, for an area of $1 \times 1\ \mu m^2$.

Fig. 1(g) and (h) exhibit the SE extracted wavelength-dependent optical constants (*n* and *k*) for the YDH, HfO_2, and SiO_2 thin films. It is found that *n* decreases slightly when Y_2O_3 is doped to the HfO_2 material (i.e., YDH thin films). This can be attributed to oxygen vacancies (from Y_2O_3) incorporated into the HfO_2 lattice, resulting in a reduced material density and hence in the *n* value. At a wavelength of 350 nm, for comparison, the *n* values obtained here are in excellent agreement with the results from the literature [15], [22], [29], with only deviations of $\pm 0.58\%$ for YDH, $\pm 1.12\%$ for HfO_2, and $\pm 2.55\%$ for SiO_2 thin films. By using the measured *k* values of the YDH and HfO_2 thin films, the absorption coefficient, α for each material is calculated [see Fig. 1(i)] from the following relation of $\alpha = 4\pi k/\lambda$. Subsequently, the E_g is estimated using the Tauc plot as shown in Fig. 1(j), and is found to be $\sim$6.21 and $\sim$5.76 eV for the YDH and HfO_2 thin films, respectively. The E_g value of the YDH thin films is consistent with the finding reported by Chen *et al.* which is $\sim$6.24 eV for $(Y_2O_3)_{0.26}(HfO_2)_{0.74}$ [22]. As for the HfO_2 thin films, the estimated E_g is comparable with various values reported in the literature [30]–[32]. It was assumed that the doping of Y_2O_3 changes the chemical element, i.e., electron states (from Hf-O-Hf to Hf-O-Y) [21], and furthermore introduces charge defects that increase the E_g of HfO_2 material [33]. This has been shown using the first-principles calculation that by adding Y_2O_3 to the HfO_2 material, the highest occupied defect level will fall into the valence band rather than the energy gap, which explains the E_g broadening [33]. The E_g can also be affected by the microstructure of the films. It has been shown that the degree of crystallinity for YDH thin films can be improved (from amorphous to polycrystalline) for $>8\%$ doping of Y_2O_3 into the HfO_2 material [21]. This can be examined from the AFM surface scans shown in Fig. 1(d) and (e) for the YDH and HfO_2 thin films, respectively. Irregular nanograins can be well observed on the YDH thin films which are correlated with an increase in the RMS roughness to $\sim$1.20 nm, compared to the RMS roughness of the HfO_2 thin films which is only $\sim$0.65 nm. The HfO_2 thin films exhibit more uniform surface, i.e., less and smaller nanograins, which is consistent with reported amorphous HfO_2 thin films (i.e., similar AFM image and RMS roughness $\sim$0.91 nm) [34]. A change in films microstructure can increase the E_g, as a similar behavior was observed in yttria-stabilized zirconia (YSZ) thin films [35]. Additionally, the increase in the lattice constant and the development of strain in YDH thin films can also increase the E_g [20].

The increase in E_g that results in lower α and *k* values, indicates the transparency of the YDH films in the UV-C wavelengths below 250 nm. This is proven by comparing the transmission measurement of the YDH and HfO_2 thin films using spectrophotometer (see Fig. 2). Both materials were deposited at the same thickness of $\sim$30 nm on UV-grade sapphire substrates (thickness of $\sim$430 μm). The transparency of $\sim$80% in the visible regime exhibited by YDH and HfO_2 thin films is consistent

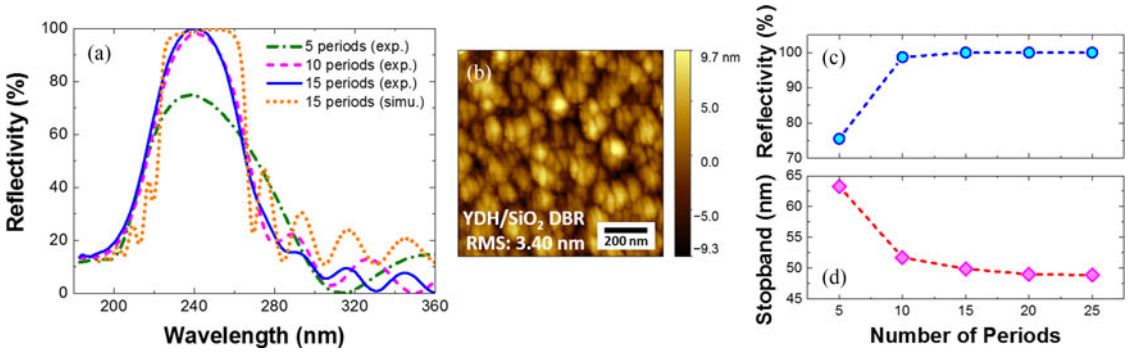

Fig. 3. YDH/SiO_2 DBR characteristics showing (a) experimental and simulated reflectivity spectra for various DBR periods, and (b) AFM surface scan for the DBR structure with 15 periods. The (c) reflectivity and (d) stopband for various DBR periods.

with the literature [21], [29], [30], [32], [36]. Focusing in the UV regime, the YDH thin films is more transparent compared to HfO_2 thin films. The absorbance spectrum (inset of Fig. 2) reveals that the YDH thin films only start absorbing drastically for wavelengths shorter than ~225 nm. In comparison, the HfO_2 thin films already show apparent absorption even in the UV-A regime. Therefore, by doping Y_2O_3 into the HfO_2 material, the newly formed YDH material is a promising candidate as the high RI layer for forming a UV-C dielectric DBR together with SiO_2 as the low RI layer. Although the *n* value for the YDH decreases slightly compared to HfO_2 [as shown in Fig. 1(g)], the RI contrast is still high. Other materials being used as the high RI layer for the oxide or fluoride type UV-C DBRs (e.g., Al_2O_3 [10] and LaF_3 [13]) have even lower *n* values (>20% reduction). This resulted in insufficient RI contrast and thus a high number of periods (>40 periods) were required to achieve >99% reflectivity [13].

4. Design and Characterizations of DBRs

Next, various YDH/SiO_2 DBRs were deposited on UV-grade sapphire substrates with a target center wavelength of 240 nm. The thickness of each layer in the DBR was designed at quarter-wavelength and the deposition was calibrated with SE measurements. The number of periods deposited was varied from 5 to 25 to compare the reflectivity and stopband of the DBR. The reflectivity measurements were performed using a spectrophotometer equipped with an integrating sphere and baselined with a UV certified MgF_2-coated Al mirror. By applying the measured *n* and *k* values for each material, the transfer-matrix method (TMM) simulations were used to calculate the reflectivity spectrum and required layer thickness. The DBR stopband is approximated by [37]

$$\frac{\Delta\lambda}{\lambda_o} = \frac{4}{\pi}\arcsin\left(\frac{n_1 - n_2}{n_1 + n_2}\right) \tag{1}$$

where λ_o is the center wavelength, n_1 is the high RI, and n_2 is the low RI. Fig. 3(a) shows the experimental reflectivity spectra for YDH/SiO_2 DBRs of 5, 10 and 15 periods. The simulated reflectivity spectrum for 15 periods DBR is also shown for comparison. The reflectivity spectra of the experiment and simulation for YDH/SiO_2 DBR with 15 periods show good agreement in terms of the reflectivity peak and position of the spectrum. However, the stopband of the experimental spectrum is slightly narrower than in the simulation result. This might arise from a smaller RI contrast in the actual case when taking into account the optical loss from material absorption and interface scattering.

Fig. 3(b) shows the AFM surface scan of the 15 periods YDH/SiO_2 DBR. The RMS roughness is ~3.40 nm, which is rougher than the single layer films of YDH and SiO_2 shown in Fig. 1. The increase in RMS roughness is associated with the interface roughness in the DBR stack, as evidenced in the cross-sectional SEM shown in the inset of Fig. 4. These imperfect interfaces can introduce

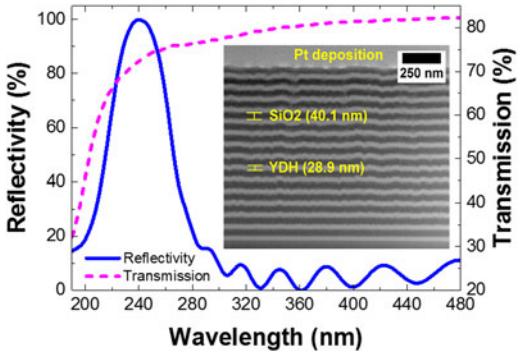

Fig. 4. The reflectivity spectrum for 15 periods YDH/SiO_2 DBR and the transmission spectrum for a ~29 nm thick YDH thin films. The inset shows the cross-sectional SEM of the DBR structure.

scattering loss to the DBR, which can degrade the device performance (e.g., device efficiency of a VCSEL [38]). The absence of sideband interference fringes at shorter wavelength for the experiment spectra is due to the onset of the fundamental YDH absorption edge. Fig. 3(c) exhibits that a high reflectivity of >99.9% can be achieved with only 15 periods of YDH/SiO_2 DBR. For comparison, more than 40 periods are required for Al_2O_3/SiO_2 DBR to achieve the same reflectivity in the UV-C regime due to insufficient RI contrast [13]. Due to the high RI contrast, the stopband of YDH/SiO_2 DBR is also considered broad (i.e., ~50 nm) as shown in Fig. 3(d), which can cover an extensive spectrum of the UV-C regime. If Al_2O_3/SiO_2 DBR is used, the stopband achieved is only ~26 to 39 nm broad [13].

In Fig. 4, the reflectivity spectrum of 15 periods YDH/SiO_2 DBR is plotted with the transmission spectrum of single layer YDH thin films (thickness of a quarter-wavelength, i.e., ~29 nm). The reflectivity peak is obtained merely before the absorption of the YDH layers in the YDH/SiO_2 DBR becomes dominant. The inset of Fig. 4 shows the cross-sectional SEM micrograph of the DBR structure. The cross-sectional SEM sample was prepared using the focused-ion-beam (FIB) lift-out technique with Pt-coated on top as a protection layer during the FIB milling. The cross-sectional SEM shows a clear contrast between the individual YDH (bright) and SiO_2 (dark) layers. A homogeneous layer sequence showing uniform period thickness distribution along the growth direction (bottom-up) was observed. The thickness of the deposited YDH and SiO_2 thin films were highly precise and in excellent agreement (<1% tolerance) with the thickness calculated from the TMM simulation. As the number of periods deposited for YDH/SiO_2 DBR increases, the interfaces were less smooth due to the accumulation of strain and the roughness introduced by each layer. This can potentially be improved by further optimization of the deposition process (e.g., RF power, Ar pressure, reactive sputtering of O_2:Ar, and substrate temperature). For example, the RMS roughness decreased (from 2.97 to 2.10 nm) as the RF power was increased from 50 to 80 W during the sputtering of HfO_2 films [29]. Also, by using reactive sputtering (example mixing O_2:Ar), the RMS roughness can be reduced. It is found that a smoother surface was obtained, i.e., RMS roughness reduced from 8.61 to 4.57 nm as the O_2:Ar flow ratio increased from 0 to 0.2 for sputtered HfO_2 films [32]. All of the above approaches are applicable for minimizing the interface roughness during the sputtering of YDH/SiO_2 DBRs.

A summary of the key parameters achieved in this study is listed in Table 1. Compared with the prior reported work of other oxides-based DBRs, the YDH/SiO_2 DBR features the highest reflectivity at sub-250 nm operating wavelengths by using only 15 periods and demonstrates a broad stopband of ~50 nm. By optimizing the deposition process as mentioned above, smoother interfaces can be obtained, and higher reflectivity for the DBR can be achieved with fewer period numbers. From the fabrication point of view, in addition to the RF magnetron sputtering, the DBRs (taking HfO_2/SiO_2 DBR for example) can be fabricated using various deposition methods such as plasma ion-assisted deposition (PIAD) [15], ion plating (IP) [15], and ion-beam-assisted electron-gun vacuum evaporation [16]. Although the RI values change slightly for HfO_2 and SiO_2 when

TABLE 1
Comparison of the Performance of Oxides-Based DBRs for UV Wavelengths

Material system	Fabrication method	Period	Center wavelength (nm)	Reflectivity (%)	Stopband (nm)	Ref.
Al_2O_3/SiO_2	RF magnetron sputtering	42.5	296	99.0	26 to 39	[13]
HfO_2/SiO_2	RF magnetron sputtering	10	311	97.0	65	[13]
HfO_2/SiO_2	Plasma ion-assisted deposition	11.5	250	98.8	45	[15]
YDH/SiO_2	**RF magnetron sputtering**	**15**	**240**	**99.9**	**50**	**This work**

PIAD and IP deposition methods are used [15], the RI deviations for both materials are still $<$10%. As above discussed, the RI value of our deposited YDH films (using RF magnetron sputtering) only deviates $\pm$0.58% compared to the RI values of YDH films deposited using electron beam evaporation [22]. To compensate any significant RI variation, additional period can be deposited for the DBR to obtain the targeted reflectivity. In addition to the RI, other DBR related factors such as thickness and interface roughness can be controlled through the optimization of the fabrication process. Reveret *et al.* [16] reported that as long as the interface roughness is $<$5 nm, the DBR reflectivity remain the same. Our AFM surface-scan indicates RMS roughness of $\sim$3.40 nm for the YDH/SiO_2 DBR. Moreover, the fabricated thickness is well-controlled ($<$1% fabrication tolerance) as shown from the cross-sectional SEM.

5. Conclusion

In summary, a highly reflective $>$99.9% oxides-based DBR was demonstrated for the UV-C wavelength regime by using 15 periods of YDH/SiO_2 layers. The reflectivity spectrum was centered at $\sim$240 nm with a relatively broad stopband of $\sim$50 nm. A comparison between YDH and HfO_2 thin films was made using the SE and spectrophotometry techniques. The YDH thin films exhibited better transparency in the UV-C regime especially below 250 nm, making this material promising as the high RI layer in a DBR structure. The realization of highly reflective and broad stopband YDH/SiO_2 DBR will benefit the UV photonic devices advancement for improved device efficiency in the UV-C regime.

Acknowledgment

This research used resources of the Core Labs of KAUST.

References

[1] T. Someya, K. Tachibana, J. Lee, T. Kamiya, and Y. Arakawa, "Lasing emission from an $In_{0.1}$ $Ga_{0.9}N$ vertical cavity surface emitting laser," *Jpn. J. Appl. Phys.*, vol. 37, no. 12A, pp. L1424–L1426, 1998.
[2] J. Y. Zhang *et al.*, "Blue-violet lasing of optically pumped GaN-based vertical cavity surface-emitting laser with dielectric distributed Bragg reflectors," *J. Lightw. Technol.*, vol. 27, no. 1, pp. 55–59, Jan. 2009.
[3] Y.-S. Liu *et al.*, "Optically pumped vertical-cavity surface-emitting laser at 374.9 nm with an electrically conducting n-type distributed Bragg reflector," *Appl. Phys. Exp.*, vol. 9, no. 11, Oct. 2016, Art. no. 111002.
[4] T. T. Kao *et al.*, "Sub-250 nm low-threshold deep-ultraviolet AlGaN-based heterostructure laser employing HfO_2/SiO_2 dielectric mirrors," *Appl. Phys. Lett.*, vol. 103, no. 21, Nov. 2013, Art. no. 211103.
[5] F. Li *et al.*, "Fabrication and characterization of a room-temperature ZnO polariton laser," *Appl. Phys. Lett.*, vol. 102, no. 19, May 2013, Art. no. 191118.

[6] T. Moudakir *et al.*, "Design, fabrication, and characterization of near-milliwatt-power RCLEDs emitting at 390 nm," *IEEE Photon. J.*, vol. 5, no. 6, Dec. 2013, Art. no. 8400709.
[7] M. S. Alias *et al.*, "Enhancing the light-extraction efficiency of an AlGaN nanowire ultraviolet light-emitting diode by using nitride/air distributed Bragg reflector nanogratings," *IEEE Photon. J.*, vol. 9, no. 5, Oct. 2017, Art. no. 4900508.
[8] Z. Xie *et al.*, "AlGaN-based 330 nm resonant-cavity-enhanced p-i-n junction ultraviolet photodetectors using AlN/AlGaN distributed Bragg reflectors," *Phys. Status Solidi C*, vol. 7, nos. 7–8, pp. 1821–1824, 2010.
[9] T. Detchprohm *et al.*, "Sub 250 nm deep-UV AlGaN/AlN distributed Bragg reflectors," *Appl. Phys. Lett.*, vol. 110, no. 1, Jan. 2017, Art. no. 011105.
[10] J. Sun, X. Li, W. Zhang, K. Yi, and J. Shao, "High-reflectivity mirrors by Al_2O_3, LaF_3 and AlF_3 for 193 nm application," *Opt. Laser Technol.*, vol. 56, pp. 65–70, 2014.
[11] F. Sarto *et al.*, "Vacuum-ultraviolet optical properties of ion beam assisted fluoride coatings for free electron laser applications," *Thin Solid Films*, vol. 515, no. 7, pp. 3858–3866, 2007.
[12] S. Shuzhen, S. Jianda, L. Chunyan, Y. Kui, F. Zhengxiu, and C. Lei, "High-reflectance 193 nm Al_2O_3/MgF_2 mirrors," *Appl. Surf. Sci.*, vol. 249, no. 1, pp. 157–161, 2005.
[13] M. L. Grilli, F. Menchini, A. Piegari, D. Alderighi, G. Toci, and M. Vannini, "Al_2O_3/SiO_2 and HfO_2/SiO_2 dichroic mirrors for UV solid-state lasers," *Thin Solid Films*, vol. 517, no. 5, pp. 1731–1735, 2009.
[14] A. Gatto *et al.*, "High-performance deep-ultraviolet optics for free-electron lasers," *Appl. Opt.*, vol. 41, no. 16, pp. 3236–3241, 2002.
[15] P. Torchio, A. Gatto, M. Alvisi, G. Albrand, N. Kaiser, and C. Amra, "High-reflectivity HfO_2/SiO_2 ultraviolet mirrors," *Appl. Opt.*, vol. 41, no. 16, pp. 3256–3261, 2002.
[16] F. Réveret *et al.*, "High reflectance dielectric distributed Bragg reflectors for near ultra-violet planar microcavities: SiO_2/HfO_2 versus SiO_2/SiN_x," *J. Appl. Phys.*, vol. 120, no. 9, Sep. 2016, Art. no. 093107.
[17] E. Rauwel *et al.*, "Stabilization of the cubic phase of HfO_2 by Y addition in films grown by metal organic chemical vapor deposition," *Appl. Phys. Lett.*, vol. 89, no. 1, Jul. 2006, Art. no. 012902.
[18] Z. K. Yang *et al.*, "Structural and compositional investigation of yttrium-doped HfO_2 films epitaxially grown on Si(111)," *Appl. Phys. Lett.*, vol. 91, no. 20, Nov. 2007, Art. no. 202909.
[19] J. Y. Dai, P. F. Lee, K. H. Wong, H. L. W. Chan, and C. L. Choy, "Epitaxial growth of yttrium-stabilized HfO_2 high-k gate dielectric thin films on Si," *J. Appl. Phys.*, vol. 94, no. 2, pp. 912–915, 2003.
[20] M. N.-A.-Alam, K. Abhilash, and C. V. Ramana, "Electrical and optical properties of nanocrystalline yttrium-doped hafnium oxide thin films," *Thin Solid Films*, vol. 520, no. 21, pp. 6631–6635, 2012.
[21] X. Chen, L. Song, L. You, and L. Zhao, "Incorporation effect of Y_2O_3 on the structure and optical properties of HfO_2 thin films," *Appl. Surf. Sci.*, vol. 271, pp. 248–252, 2013.
[22] X. Chen *et al.*, "Effect of oxygen vacancies on the laser-induced damage resistance of $Y_{0.26}Hf_{0.74}O_x$ thin films," *Opt. Lett.*, vol. 39, no. 22, pp. 6470–6473, 2014.
[23] L. Mohamed *et al.*, "Optical polarization control of photo-pumped stimulated emissions at 238 nm from AlGaN multiple-quantum-well laser structures on AlN substrates," *Appl. Phys. Exp.*, vol. 10, no. 1, Jan. 2017, Art. no. 012702.
[24] S. Zhao, X. Liu, Y. Wu, and Z. Mi, "An electrically pumped 239 nm AlGaN nanowire laser operating at room temperature," *Appl. Phys. Lett.*, vol. 109, no. 19, Nov. 2016, Art. no. 191106.
[25] X.-H. Li *et al.*, "Demonstration of transverse-magnetic deep-ultraviolet stimulated emission from AlGaN multiple-quantum-well lasers grown on a sapphire substrate," *Appl. Phys. Lett.*, vol. 106, no. 4, Jan. 2015, Art. no. 041115.
[26] Z. Lochner *et al.*, "Deep-ultraviolet lasing at 243 nm from photo-pumped AlGaN/AlN heterostructure on AlN substrate," *Appl. Phys. Lett.*, vol. 102, no. 10, Mar. 2013, Art. no. 101110.
[27] M. S. Alias *et al.*, "Optical constants of $CH_3NH_3PbBr_3$ perovskite thin films measured by spectroscopic ellipsometry," *Opt. Exp.*, vol. 24, no. 15, pp. 16586–16594, 2016.
[28] G. E. Jellison and F. A. Modine, "Parameterization of the optical functions of amorphous materials in the interband region," *Appl. Phys. Lett.*, vol. 69, no. 3, pp. 371–373, 1996.
[29] B. Deng *et al.*, "Modulation of the structural and optical properties of sputtering-derived HfO_2 films by deposition power," *Opt. Mater.*, vol. 37, pp. 245–250, 2014.
[30] F. L. Martínez *et al.*, "Optical properties and structure of HfO_2 thin films grown by high pressure reactive sputtering," *J. Phys. D, Appl. Phys.*, vol. 40, no. 17, pp. 5256–5265, 2007.
[31] J. M. Khoshman, A. Khan, and M. E. Kordesch, "Amorphous hafnium oxide thin films for antireflection optical coatings," *Surf. Coat. Technol.*, vol. 202, no. 11, pp. 2500–2502, 2008.
[32] S. Jena *et al.*, "Effect of O_2/Ar gas flow ratio on the optical properties and mechanical stress of sputtered HfO_2 thin films," *Thin Solid Films*, vol. 592, pp. 135–142, 2015.
[33] G. H. Chen, Z. F. Hou, X. G. Gong, and Q. Li, "Effects of Y doping on the structural stability and defect properties of cubic HfO_2," *J. Appl. Phys.*, vol. 104, no. 7, Oct. 2008, Art. no. 074101.
[34] M. Ramzan *et al.*, "Optical characterization of hafnium oxide thin films for heat mirrors," *Mater. Sci. Semicond. Process.*, vol. 32, no. 5, pp. 22–30, 2015.
[35] S. Heiroth, R. Ghisleni, T. Lippert, J. Michler, and A. Wokaun, "Optical and mechanical properties of amorphous and crystalline yttria-stabilized zirconia thin films prepared by pulsed laser deposition," *Acta Mater.*, vol. 59, no. 6, pp. 2330–2340, 2011.
[36] A. Ortega, E. J. Rubio, K. Abhilash, and C. V. Ramana, "Correlation between phase and optical properties of yttrium-doped hafnium oxide nanocrystalline thin films," *Opt. Mater.*, vol. 35, no. 9, pp. 1728–1734, 2013.
[37] H. Li and K. Iga, *Vertical-Cavity Surface-Emitting Laser Devices*. Berlin, Germany: Springer, 2003.
[38] M. S. Alias, S. Shaari, and S. M. Mitani, "Optimization of electro-optical characteristics of GaAs-based oxide confinement VCSEL," *Laser Phys.*, vol. 20, no. 4, pp. 806–810, 2010.